A New Lensed-Fiber Configuration Employing Cascaded GI-Fiber Chips

Kazuo Shiraishi, *Member, IEEE, Member, OSA*, and Shin-Ichi Kuroo

***Abstract*—A new scheme is proposed for lensed fibers having high coupling efficiency between laser diodes and single-mode fibers with a long working distance. The new lensed fiber consists of a pair of GI-fiber tips having different focusing parameters. The measured net coupling loss between a laser diode operating at a wavelength of 1.3 μm and a single-mode fiber is as low as 1.5 dB. The working distances are around 50 μm, much longer than those of conventional lensed fibers.**

***Index Terms*—Optical fibers, optical fiber connecting, optical fiber device, lenses, semiconductor lasers, spot size.**

I. Introduction

A COMPACT and low-loss scheme for the coupling between laser diodes (LD's) and single-mode fibers (SMF's) is a basic, important technical aspect in the construction of practical fiber networks. Lensed fibers have desirable features for the coupling scheme, such as compactness, simplicity, stability, and freedom from bulky lenses [1]–[11]. Not only a low-coupling loss, but also a long working distance—the air gap between the LD and SMF—is required so that no contact occurs between the LD and SMF during the assembly process and to prevent unstable oscillation of LD's due to backward light reflected at the lensed-fiber endface. In fiber-grating external cavity lasers, for example, low loss and long working-distance characteristics are essential [12], [13].

In previous papers, lensed fibers having long working distances of more than 100 μm were reported as schematically illustrated in Fig. 1(a) and (b) [14], [15]. In the literature, the influence of light reflection from the lensed-fiber endfaces was also confirmed to be negligible. Coupling losses in these schemes, however, were not so low, typically around 4 dB. Such magnitude of loss would be acceptable in applications for low-cost arrayed coupling schemes, but much lower losses are required in light-source modules that are used for fiber amplifiers and fiber-grating lasers.

To obtain lower coupling losses, the lensed fiber should have 1) a numerical aperture (NA) as high as that of the LD at the input end and 2) an NA as low as that of the SMF at the output end. The previously proposed configurations, Fig. 1(a) and (b), satisfy the second condition, but not the first one. In conventional lensed fibers, hemispherically-ended SMF's, small (5-15 μm) hemispherical radii are employed to satisfy the first condition, and thus the working distances are restricted

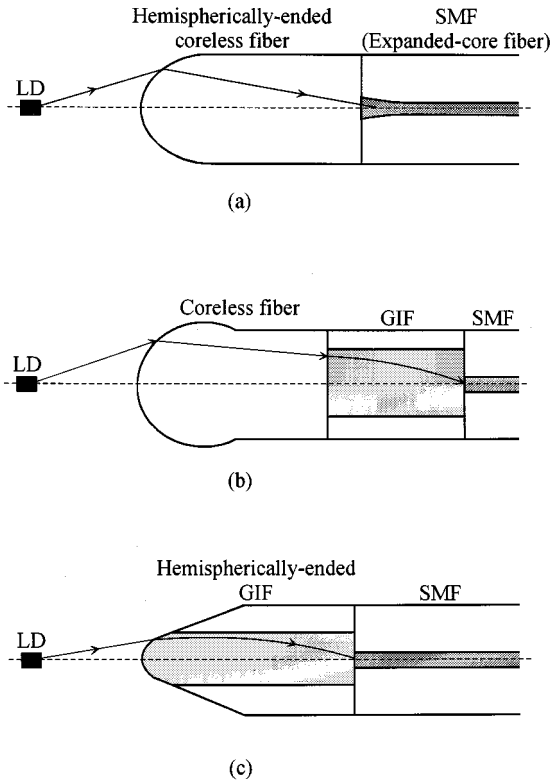

Fig. 1. Coupling between the LD and the SMF by lensed fibers employing (a) a coreless fiber and an expanded-core fiber, (b) a coreless fiber and a graded-index fiber (GIF) tip, and (c) a hemispherically-ended GIF.

to being as short as the values of the radii. Another approach that satisfies the first condition with a reasonable working distance is to employ a hemispherically ended graded-index fiber (GIF) as schematically illustrated in Fig. 1(c), which enables a long working distance of 45 μm [8]. In this case, however, the second condition is not satisfied, and thus the measured coupling loss is still relatively high (4 dB).

In the present paper, a new configuration is proposed for a lensed fiber that satisfies the above two conditions simultaneously. Simple formulas for designing the new structure are presented. The low-loss and long working-distance characteristics of the proposed configuration are experimentally verified.

II. Principle

Fig. 2 schematically illustrates the proposed structure. The new lensed fiber utilizes a hemispherically-ended GIF tip followed by another GIF tip. In the following, the focusing

Manuscript received December 8, 1999; revised March 21, 2000. This work was supported in part by a Grant-in-Aid for Scientific Research (B).

The author is with the Faculty of Engineering, Utsunomiya University, Utsunomiya 321-8585, Japan.

Publisher Item Identifier S 0733-8724(00)05082-9.

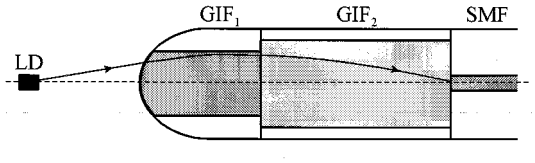

Fig. 2. Schematic illustration of the newly proposed coupling scheme that utilizes a pair of GIF tips.

properties of the conventional lensed fiber are analyzed first, and then the performance of the new configuration is presented.

The configuration of the previously proposed lensed fiber is schematically illustrated in Fig. 3(a). Calculated ray trajectories in the fiber and radial position as a function of the GIF_1 length (L_1) are shown in Fig. 3(b), in which the emission angle θ of the ray at the LD endface is used as a parameter. Typical values are assumed for structural parameters: working distance $D = 50\ \mu$m, radius of hemisphere $R = 75\ \mu$m, and refractive index of fiber cladding $n = 1.45$. The specific core radius is defined as $A_{g1} \equiv a_1(2\Delta_1)^{-1/2} = 200\ \mu$m, where a_1 is the core radius and Δ_1 the relative-index difference of the GIF_1. The inverse of A_g is the so-called focusing parameter, and standard GIF's used in fiber-communication networks have A_g of approximately 200 μm. It can be seen that rays are focused on the fiber axis near the fiber length of $L_1 = 500\ \mu$m. The figure shows that the lensed GIF has a higher effective NA compared to hemispherically-ended coreless fiber tips [8], [16]. This is due to the combination of a spherical lens effect plus the focusing effect of the GIF itself. The focusing property of the scheme, namely, the relationship between the input angle ϕ and the position h of the ray at the SMF endface, is shown in Fig. 3(c), in which the emission angle θ is plotted for every 1 degree. Owing to the strong focusing property of the GIF_1, the input angle $|\phi|$ increases rapidly as the angle θ increases, while h changes slightly. Rays that are coupled to the SMF should satisfy the conditions that h and ϕ are less than specific set values. The conditions for a standard SMF operating at a wavelength of $\lambda = 1.3\ \mu$m are indicated by the rectangular (dot-dashed) region. In this case, most of the rays emitted from the LD will not satisfy the conditions. The figure shows that emitted rays from the LD with $|\theta| > 9°$ can not be guided in the SMF, meaning that the coupling loss will be high. The focusing property shows that a low output NA in addition to a high-input NA is required for the low-loss coupling system.

It can be seen from Fig. 3(b) that there is a specific axial position (L_1 of approx. 200 μm) where rays are almost parallel to the fiber axis. This suggests that the angle $|\phi|$ can be decreased by splicing another GIF that has a low focusing property at this position, as schematically illustrated in Fig. 4(a). To confirm the effect of this NA conversion, ray trajectories and the focusing property of the new configuration are investigated. Because input angles of rays against the fiber axis of the GIF_2 are approximately 0°, the fiber length is required to be a quarter-pitch length to focus the rays on the axis. The length is given by $\pi A_g/2$ [17]. If the specific core radius of the GIF_2 is assumed as $A_{g2} = 500\ \mu$m, then the length of the fiber L_2 becomes 785 μm. Fig. 4(b) shows ray trajectories in the new

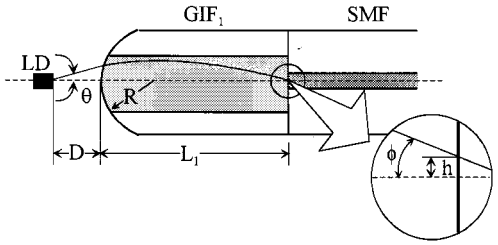

(a)

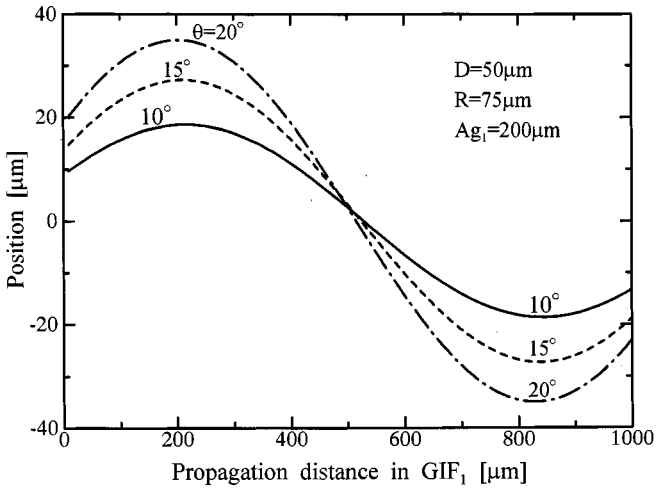

(b)

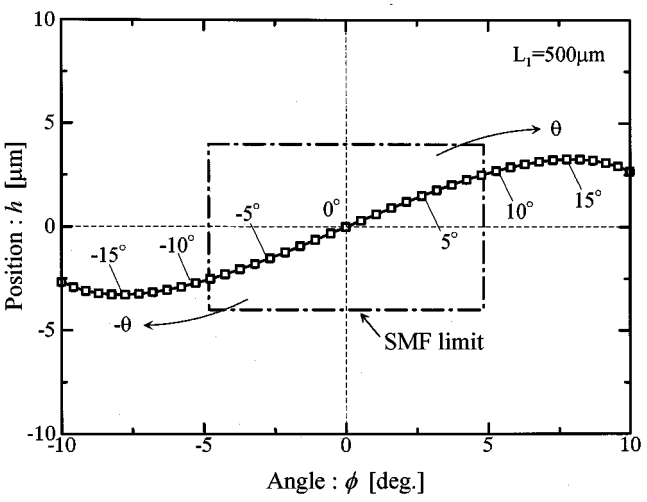

(c)

Fig. 3. Focusing properties of lensed fiber employing a single tip of GIF. (a) Definition of various parameters, (b) ray trajectories in the GIF_1, and (c) characteristics of the position h versus input angle ϕ of the ray at the input end of the SMF are shown as a function of the ray emerging angle θ (open squares) at the LD surface. The rectangular region indicated by the dot-dashed line represents the domain for specific values of h and ϕ for a standard SMF operating at a wavelength of $\lambda = 1.3\ \mu$m.

scheme, indicating that rays are focused toward the fiber axis with grazing angles. As a result, most of the rays are in the SMF limit as shown in Fig. 4(c). The figure shows that all rays

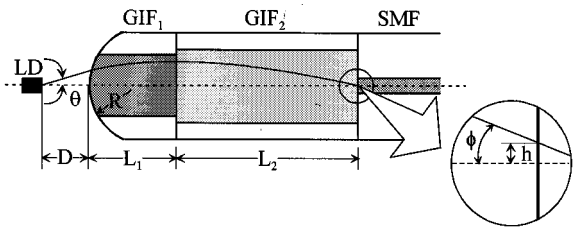

(a)

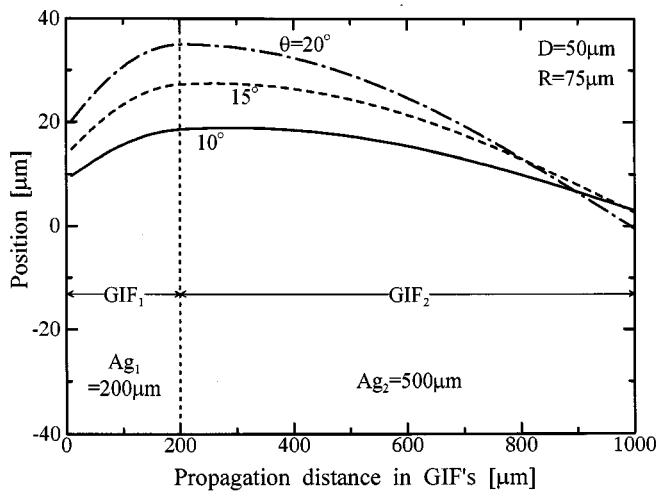

(b)

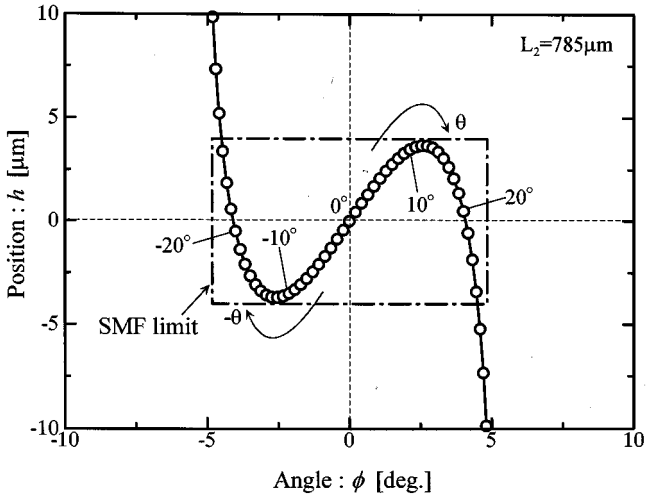

(c)

Fig. 4. Focusing properties of the new lensed fiber employing a pair of GIF tips. (a) Definition of various parameters, (b) ray trajectories in the GIF_1 and GIF_2, and (c) characteristics of the position h versus input angle ϕ of the ray at the input end of the SMF are shown as a function of the ray emerging angle θ (open circles) at the LD surface. The rectangular region represents the SMF limits as described in Fig. 3.

emitted from the LD with $|\theta| \leq 23°$ can be guided in the SMF, suggesting that coupling losses will be low. In contrast to the previous lensed fibers, the new scheme has a low-output NA in addition to high-input NA.

III. Design Considerations

To find simple and explicit expressions for determining optimum structural parameters of the new lensed fiber, an analytical approach based on the theory of Gaussian-beam propagation is given first. Numerical examples of the field distributions along the fiber axis and coupling losses as a function of the structural parameters are then given by making use of the beam-propagation method (BPM).

A. Analytical Approach

The analytical approach produces a simple and general design for the scheme, while values to be obtained are not necessarily exact. In the following, modal-field profiles in the LD and SMF are assumed to be circular-symmetric and Gaussian, unless otherwise specified. Ray matrices in the air gap (M_0), hemispherically-ended GIF_1 (M_1), and the GIF_2 (M_2) are, respectively, given by

$$M_0 = \begin{bmatrix} 1 & D \\ 0 & 1 \end{bmatrix} \tag{1}$$

$$M_1 = \begin{bmatrix} \cos\gamma_1 & A_{g1}\sin\gamma_1 \\ -\frac{1}{A_{g1}}\sin\gamma_1 & \cos\gamma_1 \end{bmatrix} \begin{bmatrix} 1 & 0 \\ -\frac{1}{R}\frac{n-1}{n} & \frac{1}{n} \end{bmatrix} \tag{2}$$

$$M_2 = \begin{bmatrix} \cos\gamma_2 & A_{g2}\sin\gamma_2 \\ -\frac{1}{A_{g2}}\sin\gamma_2 & \cos\gamma_2 \end{bmatrix} \tag{3}$$

where n is the refractive index of the fiber, and γ_1 and γ_2 are defined by

$$\gamma_1 = \frac{L_1}{A_{g1}} \tag{4}$$

$$\gamma_2 = \frac{L_2}{A_{g2}}. \tag{5}$$

According to Kogelnik's $ABCD$ law [18], [19], the spot size and the curvature of an equiphase surface at any position can be easily obtained from the matrices. The ray matrix M_{10} at the output end of the GIF_1 is given by

$$M_{10} = M_1 M_0 = \begin{bmatrix} A_1 & B_1 \\ C_1 & D_1 \end{bmatrix} \tag{6}$$

where

$$A_1 = \cos\gamma_1 - \frac{A_{g1}(n-1)}{nR}\sin\gamma_1 \tag{7}$$

$$B_1 = D\left\{\cos\gamma_1 - \frac{A_{g1}(n-1)}{nR}\sin\gamma_1\right\} + \frac{A_{g1}}{n}\sin\gamma_1 \tag{8}$$

$$C_1 = -\frac{1}{A_{g1}}\sin\gamma_1 - \frac{n-1}{nR}\cos\gamma_1 \tag{9}$$

$$D_1 = D\left(-\frac{1}{A_{g1}}\sin\gamma_1 - \frac{n-1}{nR}\cos\gamma_1\right) + \frac{1}{n}\cos\gamma_1. \tag{10}$$

The radial position h and the angle ϕ of the ray in the GIF_1 are given by utilizing the matrix as follows:

$$\begin{bmatrix} h \\ -\phi \end{bmatrix} = M_{10} \begin{bmatrix} 0 \\ \theta \end{bmatrix} = \begin{bmatrix} B_1\theta \\ D_1\theta \end{bmatrix}. \tag{11}$$

The specific position where rays become parallel $(\phi = 0)$ to the fiber axis is given by putting $D_1 = 0$, namely:

$$L_1 = A_{g1} \tan^{-1}\left\{ \frac{A_{g1}}{n}\left(\frac{1}{D} - \frac{n-1}{R}\right)\right\}. \tag{12}$$

GIF_1 length L_1 is obtained as 219 μm when $D = 50$ μm, $R = 75$ μm, $n = 1.45$, and $A_{g1} = 200$ μm. The length obtained here agrees with that deduced from the ray trajectory. A simple and explicit formula for the GIF_1 length has thus been obtained while there will be a minute error owing to the fact that the ray-matrix theory used is based on a paraxial approximation.

Because the GIF_2 serves to reduce the spot size, the input spot size (w_1), namely the output spot size of the GIF_1, has to be reduced to that of the SMF (w_{SMF}), where the spot size means spot radius defined at $1/e^2$ of the maximum of the intensity. There is a simple relation between the input and output spot sizes in a quarter-pitch length of GIF_2 as follows [17]:

$$w_1 w_{\mathrm{SMF}} = \frac{\lambda}{\pi n} A_{g2}. \tag{13}$$

The spot size w_1 can be expressed by using components of the ray matrix (M_{10}) as

$$w_1^2 = \frac{\left(\frac{\pi}{\lambda}\right)^2 w_{\mathrm{LD}}^4 A_1^2 + B_1^2}{\left(\frac{\pi}{\lambda}\right)^2 w_{\mathrm{LD}}^2} \tag{14}$$

where w_{LD} is the spot size of the beam at the LD endface. From (13) and (14), the specific core radius of the GIF_2 is given by

$$A_{g2} = n\frac{w_{\mathrm{SMF}}}{w_{\mathrm{LD}}}\sqrt{\left(\frac{\pi}{\lambda}\right)^2 w_{\mathrm{LD}}^4 A_1^2 + B_1^2}. \tag{15}$$

Because the GIF_2 has a quarter-pitch length, its length L_2 is given by

$$L_2 = \frac{\pi A_{g2}}{2}. \tag{16}$$

As a result, structural parameters L_1, A_{g2}, and L_2 are obtained explicitly. In the design of the coupling scheme, parameters λ, n, D, R, and A_{g1} are assumed first, and then L_1, A_{g2}, and L_2 are automatically determined.

Fig. 5 shows calculated spot size and curvature of the equiphase surface of the light beam as a function of the propagation distance along the fiber axis. The cross-sectional beam profile at the LD is assumed to be circular-symmetric for simplicity. Parameters $w_{\mathrm{LD}} = 1$ μm, $w_{\mathrm{SMF}} = 5$ μm, $\lambda = 1.3$ μm, $n = 1.45$, $D = 50$ μm, $R = 75$ μm, and $A_{g1} = 200$ μm are assumed, and hence the other parameters are deduced as follows: $L_1 = 219$ μm, $A_{g2} = 788$ μm, and $L_2 = 1238$ μm. It can be seen that the light beam emitted from the LD focuses at the SMF endface with a matching spot size and flat equiphase surface.

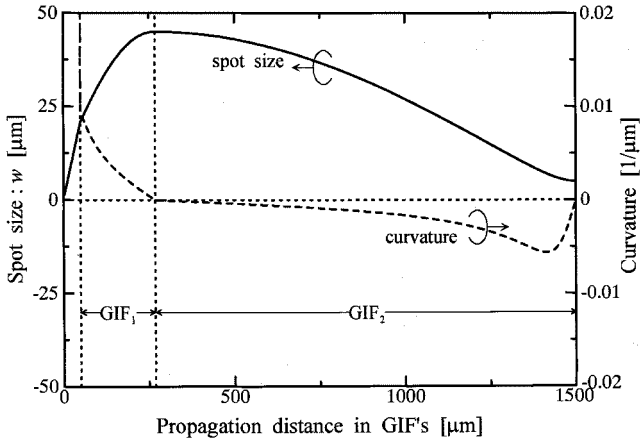

Fig. 5. Calculated spot size and curvature of the equiphase surface of the propagating beam along the axis of the lensed fiber.

B. Numerical Approach Based on the BPM

To confirm the accuracy of (12), the optimum length of GIF_1 is investigated numerically by making use of the BPM. The same parameters as in the previous section are assumed: $w_{\mathrm{LD}} = 1$ μm, $w_{\mathrm{SMF}} = 5$ μm, $\lambda = 1.32$ μm, $n = 1.45$, $D = 50$ μm, $R = 75$ μm, and $A_{g1} = 200$ μm. Not the value of A_g itself, but both the core radius and the relative-index difference have to be given specifically in the BPM simulation. Considering realistic values, the following specific parameters of GIF_1 are assumed: $\Delta_1 = 2\%$ and $a_1 = 40$ μm. Prior to the simulation, the diffraction field from the LD at the lensed fiber endface was obtained analytically to shorten the simulation time. The field distribution, intensity and equiphase surface along the lensed-fiber axis are calculated by using the BPM. The equiphase surface of the propagating beam in the GIF_1 becomes flat at the specific position, which gives the length L_1. The obtained L_1 was 217 μm, which is close to the length obtained by (12) in the previous section, namely 219 μm.

Actual LD's have noncircular-symmetric fields, and so it is preferable to assume an elliptical field for the light source when discussing the coupling losses of lensed fibers. The light emitting properties of the LD that will be used in the following analyzes and experiments are given here. The full-width at the half-maximum (FWHM) of the radiation patterns in the directions perpendicular and parallel to the junction plane are assumed as 25.0° and 19.5°, respectively [15], which correspond to a spot size at the LD surface of 1.1×1.4 μm^2.

Before finding optimum structural parameters, an example of calculated field distributions at specific points along the axis of the new lensed fiber is presented. Similar to the previous BPM simulation, the diffraction field at $D = 50$ μm from the LD at the lensed fiber endface was obtained analytically, and its intensity and equiphase surface distributions are shown in Fig. 6(a). The surface distribution is expressed by resetting the magnitude to zero when the value of the phase exceeds every 2π. It can be seen that the equiphase surface is extremely curved. The following structural parameters of the GIF_1 are assumed:

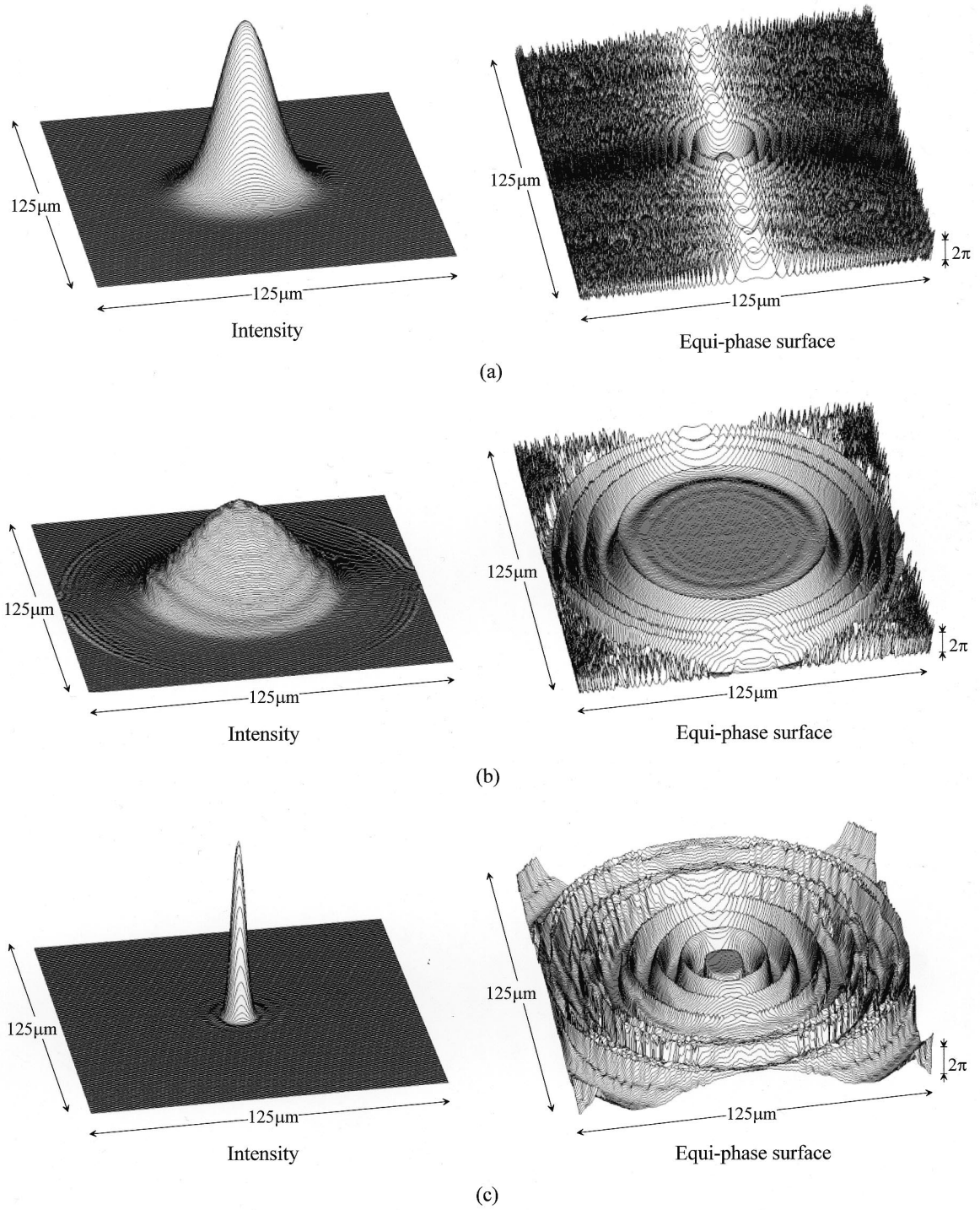

Fig. 6. Intensity and equiphase surface distributions obtained by the BPM at (a) the input end of the lensed fiber, (b) the output end of the GIF_1, and (c) the output end of the GIF_2.

$n = 1.45$, $R = 60\ \mu$m, $a_1 = 35\ \mu$m, and $\Delta_1 = 2\%$, which correspond to $A_{g1} = 175\ \mu$m. The curved surface has been flattened, except for regions of negligibly small amplitudes, after the beam propagates through the GIF_1 up to $L_1 = 171\ \mu$m as shown in Fig. 6(b). The spot diameter at the point is roughly the same as that at the input end. By making use of the spot size of the beam at this point, the parameter A_{g2} is determined from (13) so that the spot size at the output end of the GIF_2 fits that of the SMF ($w_{\mathrm{SMF}} = 5\ \mu$m). The parameter A_{g2} is thus 406 μm, and the length of the GIF_2 is determined as 638 μm from (16). In the simulation of the beam propagation in the GIF_2, specific structural parameters of $a_2 = 50\ \mu$m and $\Delta_2 = 0.758\%$ are assumed. The spot size of the beam at the output end of the GIF_1 has been reduced to match that of the SMF as shown in Fig. 6(c). The equiphase surface is almost flat within the area where the intensity is of meaningful magnitude. In this case, the coupling loss between the LD and SMF is calculated to be 0.55 dB.

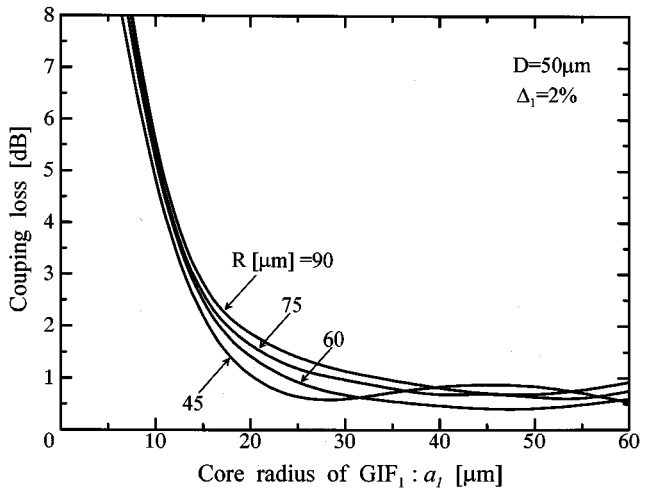

Fig. 7. Calculated coupling losses as a function of the core radius of GIF_1 for various values of hemispherical radii.

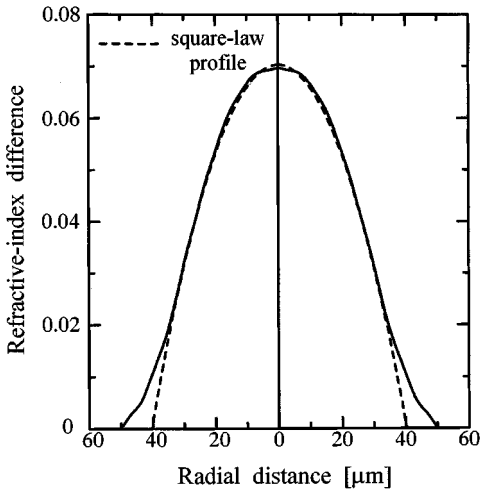

Fig. 8. The refractive-index distribution of the GIF_2. The best-fit square-law profile is shown by the dashed line.

TABLE I
STRUCTURAL PARAMETERS OF THE FIBERS USED IN THE EXPERIMENTS. THE FIGURE IN PARENTHESES REPRESENTS THE EQUIVALENT CORE RADIUS OBTAINED BY FITTING THE INDEX PROFILE WITH THE SQUARE-LAW ONE

Fiber	Core radius a [μm]	Relative-index difference Δ [%]	Specific core radius A_g [μm]
GIF_1	31.3	1.96	158
GIF_2	50.0 (40.3)	0.48	416
SMF	4.0	0.34	(step index)

In the following, optimum structural parameters of the lensed fiber are investigated. To increase the input NA of the lensed fiber, a higher relative-index difference is preferable for the GIF_1, and thus Δ_1 as high as 2% is assumed. The working distance is fixed at the relatively large value of 50 μm in the analyzes to simplify the discussions. Fig. 7 shows calculated coupling losses as a function of the core radius of the GIF_1 for various values of hemispherical radii R. In the calculation, the parameter A_{g2}, specifically Δ_2, was used as a variable parameter that changes according to Eq. (13). The loss increment for the small core radius is due to the decrement of the aperture of the GIF_1. It can be seen that lower losses are expected around $a_1 = 25$ μm at $R = 45$ μm or $a_1 = 45$ μm at $R = 60$ μm. Generally speaking, the core radius $a_1 = 40$ to 50 μm, namely $A_{g1} = 220$ μm for $\Delta_1 = 2\%$ is preferable for $R \geq 60$ μm. Low coupling losses of less than 0.5 dB with the long working distance of $D = 50$ μm would be expected in the new lensed fiber. It is noteworthy that the residual loss is mainly due to truncation of the Gaussian field by finite core radii of GIF's.

IV. EXPERIMENTS

Structural parameters of the fibers used in the experiments are listed in Table I. All fibers have a diameter of 125 μm. Due to restrictions of commercial availability, the core radius of the GIF_1 is smaller than the optimum one (45 to 50 μm).

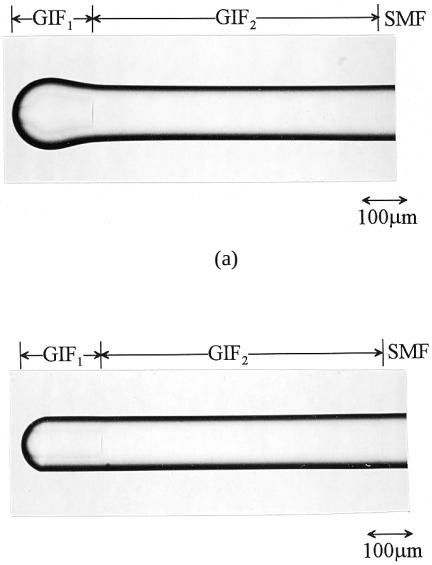

Fig. 9. Microphotographs of the fabricated lensed fibers whose endfaces were formed to hemispheric profiles by (a) arc discharge (Sample A) and (b) grinding and polishing (Sample B) processes. To display the interfaces more clearly, the sample was immersed in water, and photographs were taken under out-of-focus conditions.

TABLE II
STRUCTURAL PARAMETERS AND MINIMUM COUPLING LOSSES OF THE FABRICATED LENSED FIBERS

Sample	R [μm]	L_1 [μm]	L_2 [μm]	D [μm]	Loss [dB]
A	73	175	655	40	1.8
B	60	118	653	51	1.9

The fiber was made by the MCVD method, and the refractive-index distribution follows the square-law profile with no index dip at the center of the core. The index profile of GIF_2

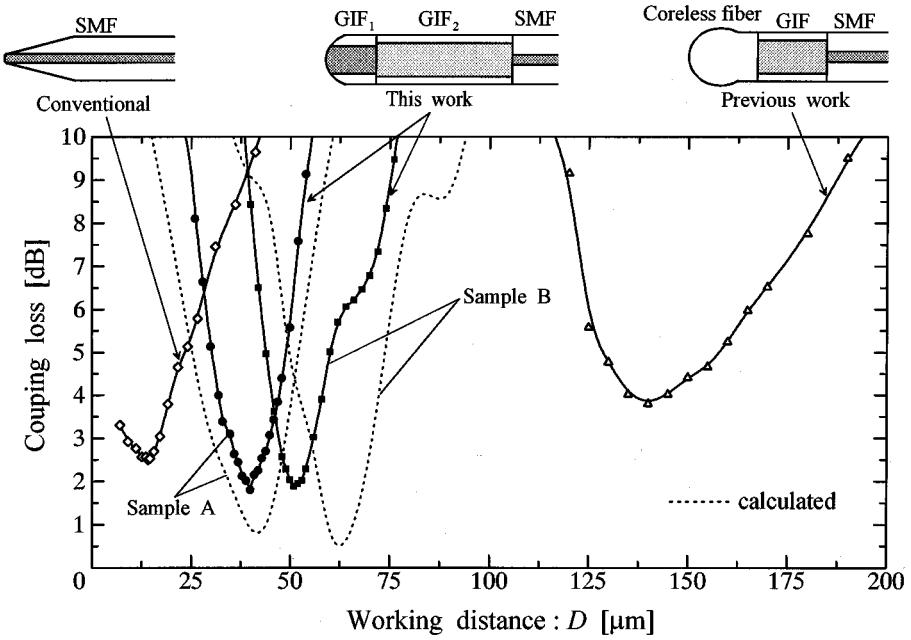

Fig. 10. Measured coupling-loss characteristics as a function of the working distance for (a) Sample A and (b) Sample B. Losses of conventional lensed fiber made of hemispherically ended SMF and the previously presented lensed fiber are shown for comparison. The dotted lines represent the calculated coupling losses.

that was made by the VAD method, however, is significantly deformed as shown in Fig. 8, in which the profile around the center and the region near the core-cladding interface differs from the square-law profile. Thus the parameter $A_{g2}(=416\ \mu\text{m})$ of the fiber was determined by fitting the square-law profile to the real one. The best-fit profile is obtained for an equivalent core radius of $a_2 = 40.3\ \mu$m, as shown by the dashed line.

The basic process of fabricating the new lensed fiber is much the same as reported before [15]. A quarter-pitch length of GIF_2 and the GIF_1 were sequentially spliced to an SMF. The fiber lengths were determined according to the theory discussed in the previous chapter. Two methods were employed to form a hemispherical shape at the end of the GIF_1, one to melt the endface by using an arc-discharge fiber splicer (Sample A), and the other to mechanically grind and polish the endface (Sample B). No anti-reflecting material coating was applied to the endface. Fig. 9(a) and (b) shows microphotographs of Samples A and B, respectively. The refractive-index profile of GIF_1 in Sample A is significantly deformed due to the melting process. Structural parameters of fabricated lensed fibers are summarized in Table II, in which typical measured characteristics that will be discussed later are also included.

Coupling characteristics between the LD and the SMF are measured as a function of the working distance as shown in Fig. 10. The LD was the same as that used in the previous work [15]. The minimum coupling loss of Sample A is 1.8 dB at $D = 40\ \mu$m, and that of Sample B is 1.9 dB at $D = 51\ \mu$m. In spite of the index deformation, Sample A has a low coupling loss. This is attributed to the fact that the index deformation within a short propagation distance do not effect on the field intensity distribution but on the phase distribution. Deviation of the phase distribution from the optimum one can be compensated by changing the length of the GIF_1. Measured losses include reflection losses at the hemispherical endface and the output end of the SMF. Thus, the net coupling losses of the lensed fibers are lower than the measured ones by approximately 0.3 dB, confirming that the new lensed fiber has high coupling efficiency. It is also noteworthy that losses would be decreased if the GIF_2 had an ideal square-law index distribution. Coupling losses of Samples A and B calculated by using the BPM are shown by the dotted lines for comparison. To simplify the calculation, a nondeformed index profile at the melted end of the GIF_1 of Sample B, an Gaussian field with a noncircular profile at the LD endface, and the ideal square-law index profile of GIF_2 chips were assumed. It can be seen that the calculated curves are in rough agreement with the measured ones; the discrepancy is ascribed to the above assumptions.

TABLE III
MEASURED TOLERANCES AGAINST LATERAL DISPLACEMENT IN THE DIRECTIONS OF VERTICAL (PERPENDICULAR) AND HORIZONTAL (PARALLEL) TO THE JUNCTION PLANE OF THE LD

Sample	vertical [μm]	horizontal [μm]
A	± 0.49	± 0.53
B	± 0.49	± 0.52
Conventional	± 0.65	± 0.80
Previous work	± 1.07	±1.05

To clarify the difference between the proposed and conventional configurations, measurements were also taken of the coupling characteristics of a commercially available lensed fiber, a hemispherically ended SMF, and the previously proposed one as shown in the same figure. It can be seen that the new scheme has lowest losses with relatively long working

distances. The tolerances, permissible displacements for a 1-dB loss increment from the minimum, for lateral displacement in the directions perpendicular and parallel to the junction plane of the LD are measured and summarized in Table III, in which tolerances in conventional schemes are also listed for comparison. It can be seen that the tolerance of the new scheme is roughly $\pm 0.5\ \mu$m, half that of the previous configuration and 70% of that of the conventional hemispherically-ended SMF. The tolerances of the new scheme are relatively small, but are within acceptable values for practical active-alignment [20].

V. Conclusion

A new lensed fiber structure has been proposed. The new scheme utilizes the hemispherically ended first GI-fiber tip that has a high focusing parameter followed by the second tip that has a low focusing parameter. The relatively large hemispherical radius and high NA of the first tip enable a long working distance to be achieved without decreasing the coupling efficiency. The second tip serves to reduce the spot size. The net coupling loss between a laser diode operating at a wavelength of 1.3 μm and the SMF of as low as 1.5 dB was measured. The working distances were around 50 μm, much longer than those of conventional lensed fibers made of hemispherically ended SMF's. Tolerances against lateral displacement, however, were relatively small at roughly $\pm 0.5\ \mu$m. The new scheme is especially promising for the fabrication of fiber grating external cavity lasers or LD modules that require high coupling efficiency.

References

[1] L. Cohen and M. Schneider, "Microlenses for coupling junction lasers to optical fibers," *Appl. Opt.*, vol. 13, pp. 89–94, Jan. 1974.

[2] J. Yamada, Y. Murakami, J. Sakai, and T. Kimura, "Characteristics of a hemispherical microlens for coupling between a semiconductor laser and single-mode fiber," *IEEE J. Quantum Electron.*, vol. QE-16, pp. 1067–1072, Oct. 1980.

[3] L. d'Auria, Y. Combemale, C. Moronvalle, and A. Jacques, "High index microlenses for GaAlAs laser-fiber coupling," *Electron. Lett.*, vol. 16, pp. 322–324, Apr. 1980.

[4] G. Wenke and Y. Zhu, "Comparison of efficiency and feedback characteristics of techniques for coupling semiconductor lasers to single-mode fiber," *Appl. Opt.*, vol. 22, pp. 3837–3844, Dec. 1983.

[5] H. Presby and C. Giles, "Asymmetric fiber microlenses for efficient coupling to elliptical laser beams," *IEEE Photon. Technol. Lett.*, vol. 5, pp. 184–186, Feb. 1993.

[6] C. Edwards, H. Presby, and C. Dragone, "Ideal microlenses for laser to fiber coupling," *J. Lightwave Technol.*, vol. 11, pp. 252–257, Feb. 1993.

[7] H. Kuwahara, M. Sasaki, and N. Tokoyo, "Efficient coupling from semiconductor lasers into single-mode fibers with tapered hemispherical ends," *Appl. Opt.*, vol. 19, pp. 2578–2583, Aug. 1980.

[8] K. Mathyssek, R. Keil, and E. Klement, "New coupling arrangement between laser diode and single mode fiber with high coupling efficiency and particulary low feedback effect," in *Proc. 10th Eur. Conf. Optical Commun.*, 1984, Paper 10A5.

[9] W. Bludau and R. Rossberg, "Low-loss laser-to-fiber coupling with negligible optical feedback," *J. Lightwave Technol.*, vol. LT-3, pp. 294–302, Apr. 1985.

[10] K. Shiraishi, "New scheme of coupling from laser diodes to single-mode fibers: A beam expanding fiber with a hemispherical end," *Opt. Lett.*, vol. 29, pp. 3469–3467, Aug. 1990.

[11] K. Kawano, *Introduction and Application of Optical Coupling Systems to Optical Devices*. Tokoyo, Japan: Gendai Kogakusha, 1991, ch. 3.

[12] T. Takagi, T. Kato, G. Sasaki, A. Miki, S. Inano, K. Iwai, A. Hamakawa, and M. Shigehara, "Fiber grating external-cavity laser diode module for 2.5 Gb/s dense WDM transmission," in *Proc. Tech. Dig. ECOC'98*, Madrid, Spain, Sept. 1998, pp. 81–82. .

[13] F. Gall, S. Mottet, N. Devoldere, and J. Landreau, "External cavity laser for DWDM access network," in *Proc. Tech. Dig. ECOC'98*, Madrid, Spain, Sept. 1998, pp. 285–286. .

[14] K. Shiraishi, N. Oyama, K. Matsumura, I. Ohishi, and S. Suga, "A fiber lens with a long working distance for integrated coupling between laser diodes and single-mode fibers," *J. Lightwave Technol.*, vol. 13, pp. 1736–1744, Aug. 1995.

[15] K. Shiraishi, H. Ohnuki, N. Hiraguri, K. Matsumura, I. Ohishi, H. Morichi, and H. Kazami, "A lensed-fiber coupling scheme utilizing a graded-index fiber and a hemispherically ended coreless fiber tip," *J. Lightwave Technol.*, vol. 15, pp. 356–363, Feb. 1997.

[16] R. Ishikawa, H. Honmou, H. Ueno, and M. Kobayashi, "Maked low-loss coupling of laser diode to single mode fiber by a plan-convex graded-index rod lens," in *Proc. Tech. Dig., IOOC-ECOC*, Venice, Italy, Oct. 1985, pp. 637–640.

[17] K. Shiraishi, A. Ogura, and K. Matsuura, "Spotsize contraction in standard single-mode fibers by use of a GI-fiber tip with a high focusing parameter," *Photon. Technol. Lett.*, vol. 10, pp. 1757–1759, Dec. 1998.

[18] H. Kogelnik, "Imaging of optical modes—Resonators with internal mirrors," *Bell Syst. Tech. J.*, vol. 44, pp. 455–494, Mar. 1965.

[19] ——, "On the propagation of Gaussian beams of light through lenslike media including those with a loss or gain variation," *Appl. Opt.*, vol. 4, pp. 1562–1569, Dec. 1965.

[20] S. Sasaki, K. Miura, T. Inoue, and M. Yano, "Hybrid integration of laser array and optical fiber array on silicon waferboard," , Aug. 1994. Tech. Rep. IEICE, Paper OPE94-38.

Kazuo Shiraishi (M'94) was born in Saitama, Japan, in 1950. He received the B.E. degree in electronics engineering from Utsunomiya University, Utsunomiya, Japan, in 1975 and the M.E. and Dr. Eng. degrees in electrical communication engineering from Tohoku University, Sendai, Japan, in 1977 and 1980, respectively.

From 1980 to 1990, he was a Research Associate at the Research Institute of Electrical Communication, Tohoku University, Sendai, and he was an Associate Professor from 1990 to 1991. He was engaged in the research on special fibers (TEC fiber), integrated optics, magnetooptic effects, optical isolators, and microfabrication processes. In 1991, he joined Utsunomiya University, Utsunomiya, Japan, where he is now a Professor. His current research interests are in the field of microoptic devices, such as laminated polarization splitters (LPS's), isolators, artificial optical materials, and special fibers, such as TEC, spot-size contracting, graded-index oval core (GIO), and lensed fibers.

Dr. Shiraishi is a member of the Institute of Electronics, Information, and Communications Engineers (IEICE) of Japan, the Magnetics Society of Japan, the Japan Society of Applied Physics, the Optical Society of America (OSA), and the International Society for Optical Engineering (SPIE).

Shin-Ichi Kuroo was born in Tochigi, Japan, in 1975. He received the B.E. degree in electrical and electronic engineering from Utsunomiya University, Utsunomiya, Japan, in 1998. He is currently working toward the M.E. degree in electrical and electronic engineering at Utsunomiya University.

His research has been concerned with efficient coupling between laser diodes and single-mode fibers.

Mr. Kuroo is a member of the Institute of Electronics, Information and Communications Engineers (IEICE) of Japan.